

Magnetic structures produced by the fluctuation dynamo

S. Louise Wilkin,* Carlo F. Barenghi, and Anvar Shukurov

School of Mathematics and Statistics, University of Newcastle, Newcastle upon Tyne, NE1 7RU, UK

(Dated: February 14, 2019)

Fluctuation dynamo action has been obtained for a flow previously used to model fluid turbulence, where the sensitivity of the magnetic field parameters to the kinetic energy spectrum can be explored. We apply quantitative morphology diagnostics, based on the Minkowski functionals, to magnetic fields produced by the kinematic fluctuation dynamo to show that magnetic structures are predominantly filamentary rather than sheet-like. Our results suggest that the thickness, width and length of the structures scale differently with magnetic Reynolds number as $R_m^{-2/(2-s)}$ and $R_m^{-0.55}$ for the former two, whereas the latter is independent of R_m , with s the slope of the energy spectrum.

PACS numbers: 47.65.-d, 07.55.Db, 02.40.Pc

The fluctuation (or small-scale) dynamo is a turbulent dynamo mechanism where a random flow of electrically conducting fluid generates a random magnetic field with zero mean value (the other type of dynamo relies on deviations of the flow from mirror symmetry and produces mean magnetic fields). A necessary condition for the fluctuation dynamo is that the magnetic Reynolds number R_m is large enough that the random velocity shear dominates over the effects of the fluid's electric resistivity. Here $R_m = ul/\eta$ where u and l are a typical velocity and length-scale respectively and η is the magnetic diffusivity. The critical value of the magnetic Reynolds number, $R_{m,cr}$, is 30–500, depending on the nature of the flow [1, 2, 3, 4, 5, 6]. Numerical simulations of the nonlinear, saturated states of the fluctuation dynamo have been reviewed in ref. [6], but more insight can be gained by a more careful analysis of the kinematic regime where the magnetic field is still too weak to affect the flow which generates it. In particular, the turbulent inertial range is undeveloped for the modest values of the Reynolds number achievable in direct numerical simulations; therefore, numerical results are often ambiguous or difficult to interpret.

Here we study the kinematic fluctuation dynamo by solving numerically the induction equation

$$\frac{\partial \mathbf{B}}{\partial t} = \nabla \times (\mathbf{u} \times \mathbf{B}) + \eta \nabla^2 \mathbf{B}, \quad \nabla \cdot \mathbf{B} = 0, \quad (1)$$

for the magnetic field \mathbf{B} in a prescribed flow $\mathbf{u}(\mathbf{x}, t)$. Unlike other numerical models of the fluctuation dynamo, our choice of the velocity field allows us to control fully its energy spectrum and time variation. We use a spectral model for \mathbf{u} , specified in Eq. (2), which was developed as a Lagrangian model of turbulence and contains its essential features: it is three dimensional, time-dependent, multi-scale, exhibits any desired energy spectrum and has transport properties (two-particle dispersion, etc.) which agree remarkably well with those of turbulent flows [7, 8] in both experiments and numerical calculations. These qualities make flows of this type attractive for applications in many fields, including atmospheric and super-

fluid turbulence [9, 10], but the model has never before been used to drive a dynamo. Given $\phi_n = \mathbf{k}_n \cdot \mathbf{x} + \omega_n t$, the velocity field \mathbf{u} is given by

$$\mathbf{u}(\mathbf{x}, t) = \sum_{n=1}^N \left[\mathbf{C}_n \times \hat{\mathbf{k}}_n \cos \phi_n + \mathbf{D}_n \times \hat{\mathbf{k}}_n \sin \phi_n \right], \quad (2)$$

where N is the number of modes and $\hat{\mathbf{k}}_n$ are randomly chosen unit vectors ($\mathbf{k}_n = k_n \hat{\mathbf{k}}_n$ is the wave vector); note that \mathbf{u} is solenoidal by construction. The *directions* of \mathbf{C}_n and \mathbf{D}_n are chosen randomly; we require, however, that they are normal to \mathbf{k}_n , so that the root mean velocity of each mode is $[(C_n^2 + D_n^2)/2]^{1/2}$.

The magnitudes of \mathbf{C}_n and \mathbf{D}_n are chosen to reproduce the desired energy spectrum, $E(k)$: $C_n = D_n = [2/3 E(k_n) \Delta k_n]^{1/2}$, where $\Delta k_n = \frac{1}{2}(k_{n+1} - k_{n-1})$ for $2 \leq n \leq N-1$, but $\Delta k_1 = \frac{1}{2}(k_2 - k_1)$ and $\Delta k_N = \frac{1}{2}(k_N - k_{N-1})$. For example, a model spectrum with suitable behaviours at $k \rightarrow 0$, $k \rightarrow \infty$ and within the inertial range $k_0 \ll k \ll k_d$, can be implemented with

$$E(k_n) = a k_n^4 \left[1 + \left(\frac{k_n}{k_0} \right)^2 \right]^{\frac{s-4}{2}} \exp \left[-\frac{1}{2} \left(\frac{k_n}{k_d} \right)^2 \right], \quad (3)$$

where k_0 corresponds to the integral scale of the flow, k_d is the dissipation wavenumber and a is the normalisation constant used to control the intensity of the flow. The Kolmogorov inertial range spectrum is obtained for $s = -5/3$. The frequencies $\omega_n = [k_n^3 E(k_n)]^{1/2}$ introduce time variation such that each mode varies at its 'eddy turnover' time.

Having specified k_0 and k_d , we can introduce the effective kinetic Reynolds number via $Re = (k_d/k_0)^{(1-s)/2}$ and $R_m = \langle u^2 \rangle^{1/2} l_0 / \eta$ for the magnetic Reynolds number, where angular brackets denote suitable averaging.

We enforce periodicity in the unit box by choosing \mathbf{k}_n randomly from a family of vectors whose components are multiples of 2π . The resulting kinetic energy spectrum $E(k)$ for $s = -5/3$ is shown in Fig. 1 (solid line), defined

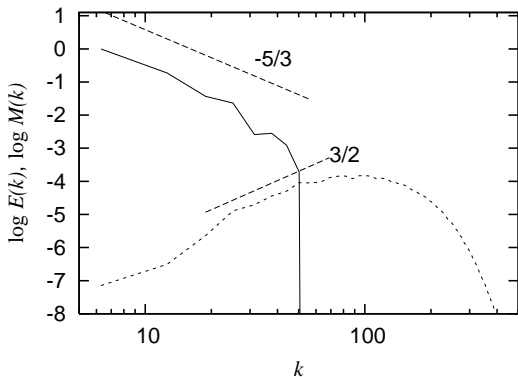


FIG. 1: Typical energy spectra for the velocity field (E , solid) and a growing magnetic field (M , dotted) in arbitrary units, with $N = 40$, $k_0 = 2\pi$ and $k_d \approx 16\pi$; this corresponds to the kinetic Reynolds number $\text{Re} \approx 16$ and $R_m \approx 2000$. Dashed lines represent power laws with the slopes indicated.

as

$$\int_0^\infty E(k) dk = \frac{1}{V} \int_V \frac{1}{2} |\mathbf{u}|^2 dV, \quad (4)$$

where V is total volume, as obtained numerically via Fourier transform of \mathbf{u} given by Eq. (2) with the input from Eq. (3). At any given time, the flow can be considered as a single realisation of a random field, but it is not random since its parameters are fixed. However, it exhibits Lagrangian chaos [7, 8], which facilitates the dynamo action. The flow is stationary on average, so we expect that the mean magnetic energy density will vary exponentially in time, $\langle B^2 \rangle^{1/2} \propto e^{\sigma t}$, with angular brackets denoting spatial averaging, with the growth (or decay) rate σ depending on R_m and the kinetic energy spectrum [3]. Meanwhile, the spatial form of the magnetic field is expected to remain statistically stationary.

We solve the induction equation (1) in a unit cubic periodic box discretised in 128^3 grid cubes. Figure 2 shows σ , measured in terms of the turnover time at the smallest velocity scale, $2\pi/\omega_n$. We see that dynamo action is initiated at the critical value $R_{m,\text{cr}} \approx 753$ for the Kolmogorov spectrum, $s = -5/3$. The data were obtained by changing R_m (or η) without changing the flow. Thus, the effective magnetic Prandtl number $P_m = R_m/\text{Re}$ varies together with R_m . Also plotted (dashed curve) is the asymptotic behaviour suggested for $R_m \gg 1$ in ref. [3]:

$$\sigma \approx \alpha \frac{U}{\mathcal{L}} \ln \left(\frac{R_m}{R_{m,\text{cr}}} \right), \quad (5)$$

where U and \mathcal{L} are a representative speed and length respectively and α is a constant of order unity; [3] obtain $\alpha \approx 2/3$ for $U = u_0$, $\mathcal{L} = 2\pi/k_0$. A very good fit to our results is achieved for a similar value $\alpha \approx 0.6$ (or ≈ 0.2 if the dissipation scale is used). The accuracy of this fit for $R_m > R_{m,\text{cr}}$ is over 96%.

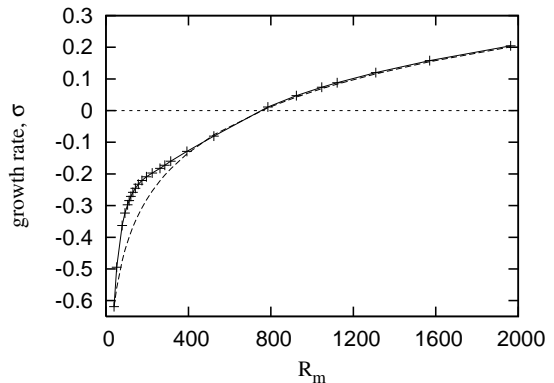


FIG. 2: The growth (or decay) rate of the r.m.s. magnetic field versus the magnetic Reynolds number for a fixed kinetic Reynolds number, for $s = -5/3$; note that $\sigma = 0$ for $R_m = R_{m,\text{cr}} \approx 753$. The dashed curve is an asymptotic fit of the form given in Eq. (5). The horizontal line $\sigma = 0$ helps to identify $R_{m,\text{cr}}$.

The energy spectrum $M(k)$ (defined similarly to Eq. (4)) of the growing magnetic field for $R_m \approx 2000$ is shown in Fig. 1 (dotted line), where it exhibits a range with $M(k) \propto k^{3/2}$ expected for a fluctuation dynamo with a single-scale random flow [1]. As we discuss below, our model also reproduces all other known features of the fluctuation dynamo that we have tested.

Asymptotic solutions of the induction equation for $R_m \gg 1$ relevant to the fluctuation dynamo have been interpreted as indicating that magnetic field is mostly concentrated into filaments of thickness $l_\eta = l_0 R_m^{-1/2}$ (for a single-scale flow) [2] or $l_\eta = l_0 R_m^{-2/(1-s)}$ for a flow with kinetic energy spectral index s [3, 4]. However, more recent numerical simulations appeared to be better consistent with magnetic sheets and ribbons [5, 6]. The latter conclusion was based on the visual inspection of magnetic isosurfaces and application of heuristic morphology indicators. Here we apply mathematically justified morphology quantifiers, based on the Minkowski functionals [11], to isosurfaces of magnetic energy density similar to those shown in Fig. 3. In an astrophysical context, this tool has been applied to galaxy distribution and cosmological structure formation [12, 13, 14].

The morphology of structures in three dimensions can be fully quantified using the four Minkowski functionals:

$$\begin{aligned} V_0 &= \iiint dV, & V_1 &= \frac{1}{6} \iint dS, \\ V_2 &= \frac{1}{6\pi} \iint (\kappa_1 + \kappa_2) dS, & V_3 &= \frac{1}{4\pi} \iint \kappa_1 \kappa_2 dS, \end{aligned} \quad (6)$$

where integration is performed over the volume and surface of the structures, respectively, and κ_1 and κ_2 are the principal curvatures of the surface. A convenient algorithm to compute the Minkowski functionals is dis-

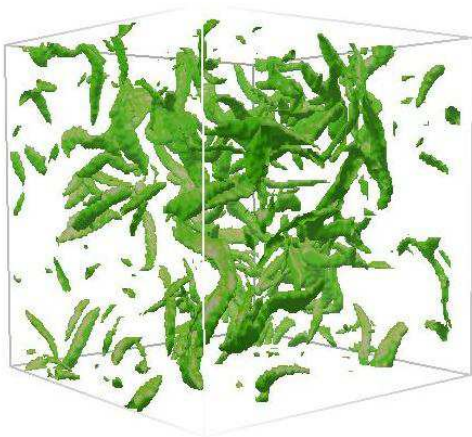


FIG. 3: (color online) The $B^2 = 3\langle B^2 \rangle$ isosurfaces of the energy density of a growing magnetic field for $R_m = 1570.5$, for the flow of Fig. 1.

cussed in refs. [13, 14]. The Minkowski functionals can be used to calculate the typical thickness, width and length of the structures, as $T = V_0/2V_1$, $W = 2V_1/\pi V_2$, and $L = 3V_2/4V_3$, respectively. Then, useful dimensionless measures of ‘planarity’ P , and ‘filamentarity’ F [12] can be defined as

$$P = (W - T)/(W + T), \quad F = (L - W)/(L + W). \quad (7)$$

In idealised cases and for convex surfaces, values of P and F lie between zero and unity. For example, an infinitely thin pancake has $(P, F) = (1, 0)$, a perfect filament has $(P, F) = (0, 1)$, whereas $(P, F) = (0, 0)$ for the sphere. Some examples are shown on the right-hand side of Fig. 4. We note that T , W and L are not necessarily such that $T < W < L$. For example, the unit cube has $T = 3/4$, $W = 2/\pi$, $L = 1/2$. Deviations from the ordering $T < W < L$ are relatively rare for random fields studied here. Nonetheless, to avoid confusion we introduce the notation $l_1 = \min(T, W, L)$, $l_2 = \text{med}(T, W, L)$ and $l_3 = \max(T, W, L)$.

As shown in Fig. 4, F increases faster than P with R_m , so the magnetic structures produced by the fluctuation dynamo are better described as filaments, especially at the larger values of R_m .

Using the Minkowski functionals, we can also reliably measure the characteristic length scales of magnetic structures and explore their scalings with R_m and s . In Fig. 5, we display l_1 against R_m at two instants in time for the flow with $s = -5/3$ illustrated in Fig 1. Whilst the behaviour for $R_m \ll R_{m,cr}$ shows variations in time, we observe for $R_m \gtrsim 200$ a time-independent scaling of the thickness of magnetic structures: $l_1 = 2\pi/k_\eta \sim R_m^{-3/4}$. This scaling, obtained in ref. [3] for a flow δ -correlated in time (see also ref. [4]) follows from the balance of the induction and diffusion terms in the induction equation [15]: for a flow with extended energy spectrum $E(k) \propto k^s$

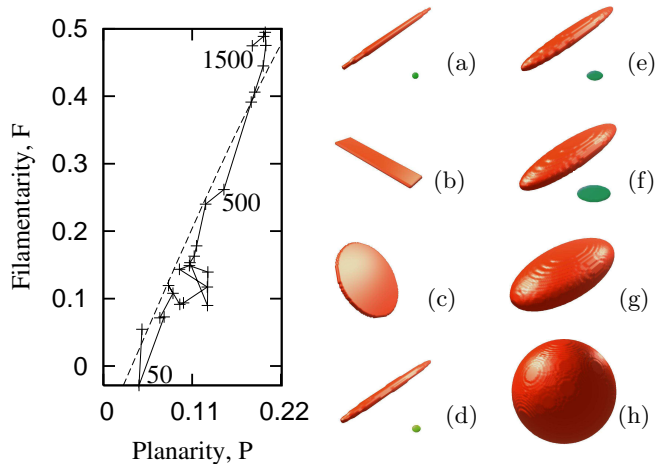


FIG. 4: (color online) The route taken by magnetic structures through the (P, F) -plane as R_m increases, averaged for each R_m between eight isosurfaces ranging from $B^2 = 1.5\langle B^2 \rangle$ to $B^2 = 5\langle B^2 \rangle$ in steps of $0.5\langle B^2 \rangle$. Three data points are labelled with their values of R_m . The dashed line illustrates the estimates of Eq. (9). The objects to the right of the figure are shown for reference: (a) filament, $(P, F) = (0.096, 0.81)$; (b) ribbon, $(P, F) = (0.66, 0.23)$; (c) pancake, $(P, F) = (0.66, 0.12)$; (d) thin cigar, $(P, F) = (0.25, 0.66)$; (e) cigar, $(P, F) = (0.18, 0.43)$; (f) fat cigar, $(P, F) = (0.14, 0.23)$; (g) rugby ball, $(P, F) = (0.087, 0.073)$ and (h) sphere, $(P, F) = (0.0036, -0.0047)$. Cross sections (in green) are also displayed for (a), (d), (e) and (f).

this yields

$$l_1 \simeq l_0 R_m^{-2/(1-s)}. \quad (8)$$

Figure 6 shows how the characteristic width l_2 and length l_3 of the magnetic structures scale with R_m . For $R_m \gtrsim 200$ we observe another time-independent scaling, $l_2 \sim R_m^{-0.55}$. This distinct behaviour of the width of magnetic structures has not been obtained in earlier analytical and numerical studies of the fluctuation dynamo. The simultaneous decrease of l_2 and l_1 , coupled with the approximately R_m -independent behaviour of l_3 (Fig. 6 inset) supports the notion that the magnetic structures become more filamentary as R_m increases (see Fig. 4). Indeed, using $l_1 \sim 2.4R_m^{-0.75}$, $l_2 \sim 0.9R_m^{-0.55}$ and $l_3 \sim 0.05R_m^0$ in Eq. (7) we can estimate, for $s = -5/3$,

$$P \sim 1 - \frac{2}{1 + \frac{3}{8}R_m^{0.2}}, \quad F \sim 1 - \frac{2}{1 + \frac{1}{18}R_m^{0.55}}, \quad (9)$$

so that $F \gg P$ for $R_m \gtrsim 200$. These relations are shown by the dashed line in Fig. 4.

To investigate how the scaling laws identified via the Minkowski functionals compare with those inferred from other measures, we calculated the inverse ‘integral scale’ of the magnetic field, $2\pi/l_I = \int kM(k) dk / \int M(k) dk$.

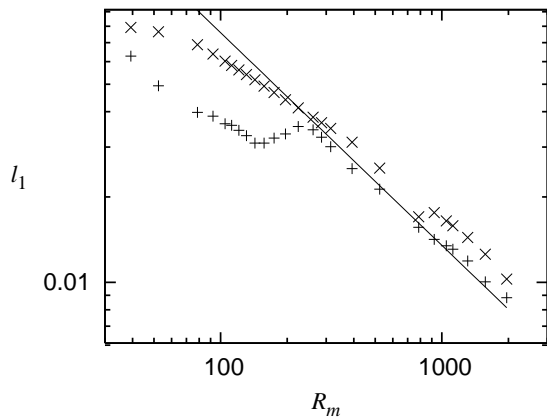


FIG. 5: Average values of the shortest dimension of the iso-surface structures (l_1) as a function of R_m at two instants in time for a flow with the energy spectrum of Fig. 1. Data marked ‘ \times ’ correspond to results attained when the smallest eddies have made 25 revolutions; ‘+’ symbols denote results at 50 rotations. The solid straight line has a gradient of $-3/4$.

We found that l_I follows a scaling of $R_m^{-0.42}$, which understandably differs from the scalings of l_1 , l_2 and l_3 . The scale l_I is a poor measure of the dimension of anisotropic magnetic structures such as filaments. We note that the above scaling of l_I is maintained for *all* subcritical and supercritical values of R_m , unlike the results of Figs. 5 and 6 which display well-defined scalings only for $R_m \gtrsim 200$. We have verified that the scaling (8) emerges for $s = -5/3, -2, -3$. On the contrary, $l_2 \sim R_m^{-0.55}$ independently of s . Asymptotic solutions [3] suggest that the fluctuation dynamo (with $\text{Pr}_m < 1$) is only possible for $s < -3/2$. Our results show that the dynamo action is possible for $s = -1$ as well, although a scaling different from (8) is exhibited. This indicates that the nature of the asymptotic solution, rather than the possibility of a dynamo, is different at $s = -1$ from that at $s < -3/2$. We also tested the proxy dimensions of ref. [16] but these do not show physically justifiable scalings.

The scaling of l_1 with R_m has been obtained [3, 4] for flows with $\text{Pr}_m = R_m/\text{Re} \lesssim 1$, where the maximum of the magnetic spectrum occurs in the inertial interval of turbulence. With the proxy Re defined above, $\text{Pr}_m > 1$ in our simulations. We cannot introduce a true Re because we do not solve the Navier-Stokes equation and therefore the kinematic viscosity is not defined in our model. The reason why scalings expected for $\text{Pr}_m \lesssim 1$ occur in our model which formally has $\text{Pr}_m > 1$ remains unclear.

In conclusion, we have shown that velocity fields of the form (2) are capable of initiating the fluctuation dynamo. This model flow reproduces many properties of turbulence and thus offers a convenient tool to study dynamos in multi-scale, well controlled flows. A quantitative and mathematically justifiable description of the morphology of magnetic structures based on the Minkowski func-

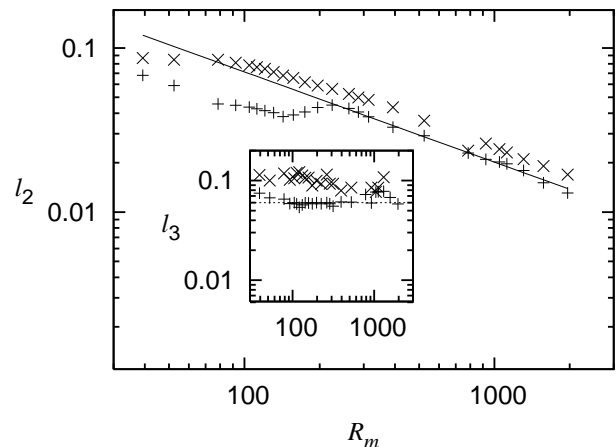


FIG. 6: As in Fig. 5, but for the width l_2 (main frame) and length l_3 (inset). The solid straight line in the main plot has a gradient of -0.55 .

tionals indicates that, at least at the kinematic stage, magnetic field is concentrated into filaments rather than sheets or ribbons. We have confirmed that the characteristic thickness of magnetic structures scales with the magnetic Reynolds number as $l_1 \propto R_m^{-2/(1-s)}$ for the energy spectrum slope of s , whereas the width varies as $R_m^{-0.55}$ and the length is independent of R_m .

We acknowledge useful discussions with S. Tobias and K. Subramanian. This work was supported by the EPSRC grant PB/KH/037026987 and the Leverhulme Trust grant F/00 125/N.

* s.l.wilkin@ncl.ac.uk

- [1] A. P. Kazantsev, Soviet Physics JETP **26**, 1031 (1968).
- [2] Y. B. Zeldovich, A. A. Ruzmaikin, and D. D. Sokoloff, *Magnetic Fields in Astrophysics* (Gordon and Breach, N. Y., 1983).
- [3] I. Rogachevskii and N. Kleeorin, Phys. Rev. E **56**, 417 (1997).
- [4] S. Boldyrev and F. Cattaneo, Phys. Rev. Lett. **92**, 144501 (2004).
- [5] A. A. Schekochihin *et al.*, Astrophys. J. **625**, L115 (2005).
- [6] A. Brandenburg and K. Subramanian, Phys. Rep. **417**, 1 (2005).
- [7] N. A. Malik and J. C. Vassilicos, Phys. Fluids **11**, 1572 (1999).
- [8] J. C. H. Fung and J. C. Vassilicos, Phys. Rev. E **57**, 1677 (1998).
- [9] D. Kivotides, J. C. Vassilicos, C. F. Barenghi, M. A. I. Khan, and D. C. Samuels, Phys. Rev. Lett. **87**, 275302 (2001).
- [10] D. Kivotides, C. F. Barenghi, and D. C. Samuels, Europhysics Letters **57**, 845 (2002).
- [11] M. A. Armstrong, *Basic Topology* (Springer, 1983).
- [12] V. Sahni, B. S. Sathyaprakash, and S. F. Shandarin, Astrophys. J. **495**, L5 (1998).
- [13] J. Schmalzing and T. Buchert, Astrophys. J. **482**, L1

- (1997).
- [14] J. Schmalzing *et al.*, *Astrophys. J.* **526**, 568 (1999).
- [15] K. Subramanian, *Phys. Rev. Lett.* **83**, 2957 (1999).
- [16] A. A. Schekochihin, S. C. Cowley, S. F. Taylor, J. L. Maron, and J. C. McWilliams, *Astrophys. J.* **612**, 276 (2004).